Algerian Journal of Research and Technology
https://doi.org/10.58681/ajrt.24080201
A.J.R.T Volume 8 (N°2) (2024) 1 - 11

Evaluation of the Effects of Dissolved CO_2 Gas on the Corrosion Rate of API 5L X60 Steel Crude Oil Pipelines, Considering the Effect of Vibration

Haider Hadi Jasim

Chemical Engineering Department, College of Engineering, Basrah University, Iraq

**Corresponding author.haider.jassim@uobasrah.edu.iq*

Received. June 17, 2024. Accepted. December 06, 2024. Published. December 20, 2024.

DOI: https://doi.org/10.58681/ajrt.24080201

Abstract. Vibrations in crude oil pipelines can occur due to the flow of crude oil, pumps, wind, earthquakes, and human activities. When vibrations are combined with corrosive environments and dissolved gases, especially CO_2, they can accelerate corrosion and ultimately lead to failure. In this study, a novel vibration immersion test was conducted in the laboratory under various temperatures and low CO_2 dissolved gas pressures to investigate the corrosion rate in API 5L X60 steel pipelines. The experimental 1991 De Waard-Lotz-Milliams correlation and a neural network method were used to evaluate the effects of CO_2 gas levels on overall corrosion rates. The results indicate that temperature, CO_2 partial pressure, and vibration directly influence corrosion rates. The corrosion rate increases uniformly at constant vibration and CO_2 partial pressure as temperature rises, exceeding 1%. At constant vibration and temperature, corrosion rates increase uniformly by less than 1% with increasing CO_2 partial pressure.

Keywords. Dissolved CO_2 gas, Vibration immersion test, Salts, ANN method, Corrosion.

INTRODUCTION

Pipeline networks are the key arteries for delivering crude oil and its products. Corrosion of pipeline networks is a significant issue in crude oil transportation. Crude oil contains various corrosive components, including water, CO_2 (g), H_2S (g), organic chlorides, organic acids, sulfur, and bacteria. Carbon dioxide (CO_2) is present in oil fields at varying concentrations and is considered the primary cause of corrosion-related failures (Li et al., 2021).

The vibration of crude oil pipelines results from different sources, such as pumps, wind, crude oil flow, and its contents, especially gases (Al-Hashimy et al., 2016). Various experimental and numerical methods are used to estimate corrosion rates, but only a few can be applied in the case of vibration effects. The most suitable method for incorporating the effect of vibration is immersion testing (Jones, 1996).

Several studies and models on the CO_2 corrosion process have been developed, but most neglect the effect of vibration phenomena on corrosion rates.

De-Waard and Lotz (1993) developed a semi-empirical model for CO_2 corrosion rates, which simulates the impact of dissolved CO_2 gas and operating conditions on corrosion rates.

Nesic et al. (1997) used a neural network approach to develop a CO_2 corrosion rate model, demonstrating that their model's extrapolation capabilities were comparable to other models.

Kermani et al. (2003) studied the corrosion process of dissolved CO_2 gas and showed that CO_2 partial pressure, concentrations of corrosive species, temperature, and pH levels are the main factors influencing CO_2 corrosion.

Dai et al. (2012) demonstrated that interactions between the pipe walls, supports, and the fluid flowing through the pipe are the primary causes of vibrations. It was found that the maximum allowable vibration amplitude for process pipelines is 0.2 mm at a maximum frequency of 40 Hz.

Amarasinghe et al. (2021) studied CO_2 dissolution and convective mixing in oil under realistic reservoir temperature and pressure conditions. They found that CO_2 dissolution in oil or water leads to oil swelling, viscosity changes, and wettability alteration.

In this paper, the vibration-induced corrosion of API 5L X60 steel pipelines is studied in the presence of dissolved CO_2 gas. Tests were conducted at various temperatures and low CO_2 pressures using an experimental immersion test on a vibrating pipeline. The results of the static immersion test were then compared with those of the vibration immersion test.

MATERIAL AND CRUDE OIL SOLUTION

Commercial API 5L X60 steel pipelines were used in southern Iraq to transport crude oil from various oil fields to the port of Basrah for export. The specimens used for immersion testing have dimensions of 50 × 25 × 5 mm, in accordance with ASTM G31 (1999). A total of 80 specimens were tested under both static and vibration conditions. The chemical composition of the API 5L X60 steel pipeline is listed in Table 1.

Table 1. Chemical composition of API 5L X60 steel pipeline (Guang, 2018).

Elements	C	Si	Mn	P	S	V	Nb	Ti	Fe
%	0.16	0.45	1.65	0.02	0.01	0.08	0.05	0.04	Balance

The crude oil samples for testing were taken from the South Rumaila oil fields in southern Iraq. Table 2 presents the physical properties and dissolved gases obtained from the field laboratory. Table 3 shows the specific gravity measured in the laboratory at different temperatures and pressures after injecting CO_2 gas into the oil solution.

Table 2.Physical properties of South Rumaila crude oil.

Propertie	API	Sulfure	Water content	Asphalt	pH	TAN	H_2S	CO_2	O_2	NaCl
			%			mgKOH/gm oil		(g)		
Value	30.2	2.92	0.75	1.45	5.8	0.112	1	0.96	0.96	13

Table 3.Measured specific gravity (ν) of South Rumaila crude oil.

Temperature (^oC)	Specific gravity as received	Specific gravity at different pressure (MPa)			
		0.2	0.4	0.6	0.8
30	0.8973	0.8672	0.8523	0.8410	0.8317
35	0.8851	0.85731	0.8484	0.8402	0.8306
40	0.8707	08420	0.8351	0.8244	0.8176
45	0.8648	0.8315	0.8242	0.8201	0.8105

IMMERSION VIBRATION CORROSION TEST METHOD

Fig. 1 shows a schematic diagram of the immersion equipment system and apparatus assembled in the laboratory according to ASTM-G32-03 (Gatto et al., 2023). The apparatus consists of a water bath equipped with a shaker. A thermocouple was used to measure the temperature of the solution during the test. A vibration meter was used to measure the vibration. The vibration meter, model HHVB82, was manufactured by Omega Engineering, Stamford, CT, China, while the thermocouple used is a 2-Channel Dual Handheld digital thermocouple manufactured by Harold G. Schaevitz Industry LLC, USA. The 500 ml capacity beakers were fixed on the heater plates and filled with a crude oil solution. A CO_2 gas container was used to supply CO_2 gas during the test.

The immersion test was conducted at temperatures of 30, 35, 40, and 45°C, over a 180-day exposure period. At the tested temperatures, the corrosion mass loss was recorded over a total of 180 days at specific intervals of 15 days. One liter of water was mixed with 50 g of sodium hydroxide and 200 g of zinc dust and boiled to create the cleaning solution (ASTM G1-90). The sample was removed from the oil solution, washed with kerosene to eliminate any remaining crude oil, and then submerged in the cleaning solution for 1 minute to remove the oxidation layer. The specimens were air-dried at room temperature. The specimens were then weighed, and their mass loss was recorded. The corrosion rate (Cr) was calculated by assuming uniform corrosion over the surface of the specimen as follows (Gatto et al., 2023):

$$C_r = \frac{W*K}{\rho\, A\, t} \qquad (1)$$

Where, $K = 8.76*10^4$ for C_r in mm/year, ρ is the mass density of steel in kg/m^3, A is the total surface area of specimen cm^2 and t is time of immersion in hr.

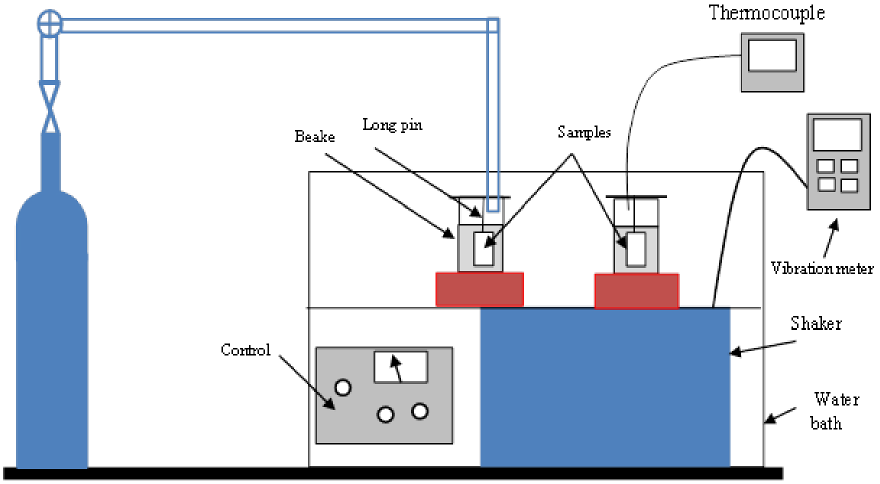

Fig 1.Schematic diagram of the immersion test apparatus.

ARTIFICIAL NEURAL NETWORKS

Artificial neural networks (ANNs) mimic certain fundamental aspects of brain function (Mamoon et al., 2023). A neuron is the basic unit of a neural network, and its shape and size may vary depending on its function (Christopher, 2010).

The simplest neural network consists of neurons, inputs, weights, a summation function, an activation function, and an output. The summation function calculates the neuron's net input, as given in Eq. (2).

$$NET_i = \sum_{j=1}^{n} W_{ij}X_j + W_{bi} \quad (2)$$

Where, NET_i : the weighted sum of the input to the *i*th processing element, *i* and *j* : the processing elements, *w*ij : the weights of the connections between *i*th and *j*th processing elements, *x*j : the output of the *j*th processing element and W_{bi} : the weights of the biases between layers.

Fig. 2 shows the structure of the ANN model used. The activation function, which processes the net input of the neuron, defines the output of the neuron.

Several functions, such as the threshold function, step activation function, and sigmoid function, are used to define the activation function. The sigmoid function is commonly used for the transfer function and generates a value between 0 and 1 for each value of the net input. The logistic transfer function of the ANN model used in this study is given by:

$$F(NET_i) = \frac{1}{1 + e^{NET_i}} \quad (3)$$

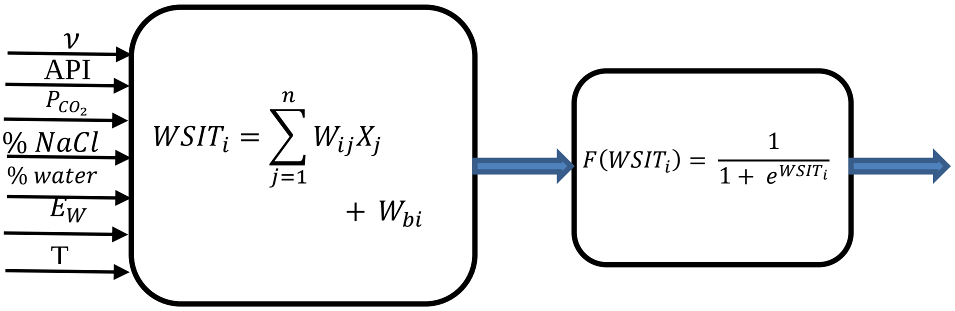

Fig 2.The structure of the ANN model.

There were seven input parameters in the network: API, P_{CO_2}, % NaCl, % water, stresses, E_W (equivalent weight), ν, and T. There was one output parameter: corrosion rate. The root mean square error (RMSE) and the correlation coefficient (R^2) values were used for comparison (Lin et al., 2017) as follows:

$$RMSE = \left[\left(\frac{1}{p}\right)\sum_j \left|t_j - o_j\right|^2\right]^{1/2} \quad (4)$$

$$R^2 = 1 - \left(\frac{\sum_j (t_j - o_j)^2}{\sum_j (o_j{}^2)}\right) \quad (5)$$

Where, *t* is the goal value, *o* is the output value, and *p* is the number of samples.

The determination of the optimal number of neurons in the hidden layers of the model is presented in Table 4. Trials were conducted using the Levenberg–Marquardt (LM) learning algorithm. According to Table 4, the optimal configuration for the input, hidden, and output layers is 7-13-1.

Table 4. The optimal number of neurons in hidden layers obtained from ANN model.

Learning algorithm	Number of neurons	Training data		Testing data	
		RMSE	R^2	RMSE	R^2
LM	7-10-1	0.1043	0.9632	0.0930	0.9540
LM	7-11-1	0.1047	0.9678	0.0962	0.9483
LM	7-12-1	0.0944	0.9555	0.0931	0.9644
LM	**7-13-1**	**0.0845**	**0.9110**	**0.0882**	**0.9514**
LM	7-14-1	0.0946	0.9473	0.0931	0.9453
LM	7-15-1	0.0959	0.9337	0.0945	0.9588
LM	7-16-1	0.0924	0.9550	0.0950	0.9633
LM	7-17-1	0.0980	0.9588	0.0828	0.9623
LM	7-18-1	0.1075	0.9578	0.0910	0.9468
LM	7-19-1	0.1081	0.9589	0.0942	0.9394

The 1991 De Waard-Lotz-Williams Correlation

The 1991 correlation is essentially similar to the 1975 equation in terms of formulation and variables, with the exception of the fugacity term, *f*(CO_2), which replaces the previous carbon dioxide partial pressure term, *P*(CO_2). The equation is stated as follows (De Waard et al., 1991):

$$\log C_r = 5.8 - \frac{1710}{T+273} + 0.67\ \mathrm{Log}(\ f_{CO_2} \quad (6)$$

Where, T is temperature in (K) and f_{CO_2} is CO_2 fugacity in (MPa). In this paper the Peng-Robinson equation of state was used for calculating the fugacity coefficient of CO_2 dissolved in crude oil (Elliott and Carl, 2012).

A summary of the results from the 1991 De Waard-Lotz-Williams correlation, the ANN model, and the static immersion experimental test is presented in Figs. 3, 4, 5, 6, 7, and 8, respectively. As shown in Table 2, the crude oil has an acid value of 0.112 mg $KOH \cdot g^{-1}$, indicating low acidity. Initially, the crude oil has a pH of 5.8. The change in pH results from CO_2 dissolving in the water present in the crude oil. As CO_2 dissolves in water, it forms carbonic acid, which increases the acidity of the crude oil solution. This process is described by Palmer et al. (1983):

$$H_2O \Leftrightarrow H^+ + OH^- \quad (7)$$

$$CO_2 + H_2O \Leftrightarrow H^+ + HCO_3^- \quad (8)$$

$$HCO_3^- \Leftrightarrow H^+ + CO_3^- \quad (9)$$

As seen in Figs. 3, 4, 5, 6, 7, and 8, with the increase in temperature and CO_2 partial pressure, the corrosion rate gradually increases. The main reason is that as the partial pressure of CO_2 increases, more CO_2 combines with water molecules in the solution, which increases the concentration of H_2CO_3 and intensifies its ionization. As a result, the concentration of H^+ ions in the solution increases, leading to a decrease in pH and an acceleration of the corrosion reaction, ultimately causing an increase in the corrosion rate.

The corrosion rate results from the effects of dissolved CO_2 gas in crude oil, contributing significantly to the total immersion corrosion rate, as seen in Figs. 2–8.

For pressures of 0.2, 0.4, 0.6, and 0.8 MPa at T = 30°C, the percentage rates are 15.89% (0.0110/0.0692 × 100%), 17.40% (0.0120/0.0692 × 100%), and 18.18% (0.0126/0.0692 × 100%). At 0.2, 0.4, 0.6, and 0.8 MPa and T = 45°C, the corresponding values are 17.49% (0.0462/0.2641 × 100%), 17.68% (0.0467/0.2641 × 100%), and 19.27% (0.0509/0.2641 × 100%).

Figs. 9, 10, 11, and 12 show corrosion rates obtained from static and vibrational immersion tests at varying temperatures and CO_2 partial pressures. The vibration frequency was set at 40 Hz with an amplitude of 0.2 mm for all vibration tests. Based on the results, vibration increased the corrosion rate compared to static conditions. However, corrosion rates do not increase uniformly. Increasing the temperature and CO_2 partial pressure affects the corrosion rate values and leads to an increase.

The difference between static and vibrational corrosion rates in crude oil is relatively small during the first two months of immersion testing. However, this trend reverses with longer immersion times. This is due to the fact that longer immersion times result in higher corrosion reaction rates on the specimen surface, i.e., greater dissolution of the steel under the continuous attack of corrosive ions and agents, which eventually causes increased weight loss.

The results showed that the solubility of CO_2 improved with increasing pressure under vibrational conditions. Therefore, the corrosion rate is enhanced since CO_2 solubility may increase due to vibration. On the other hand, temperature plays a role in the solubility of CO_2 in crude oil. CO_2 solubility increases significantly when crude oil has low viscosity, as it is easier for CO_2 to diffuse into the oil phase as the temperature rises (Ziegler et al., 2003).

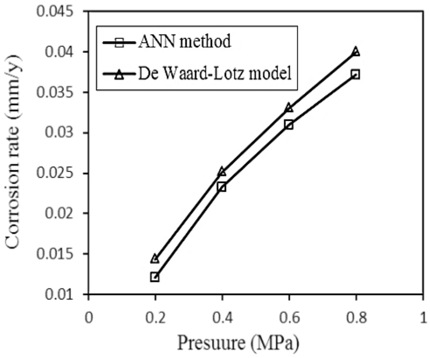

Fig. 3 Corrosion rate (mm/year) obtained from static test at 30°C.

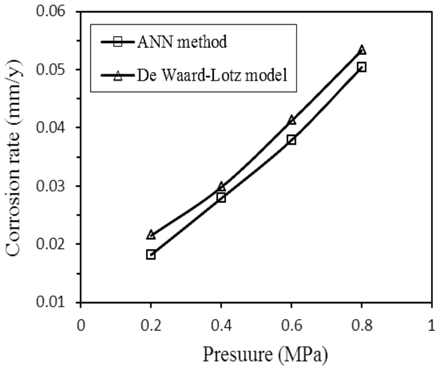

Fig. 4 Corrosion rate (mm/year) obtained from static test at 35°C.

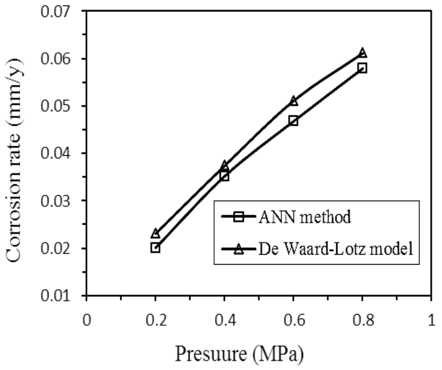

Fig. 5 Corrosion rate (mm/year) obtained from static test at 40°C.

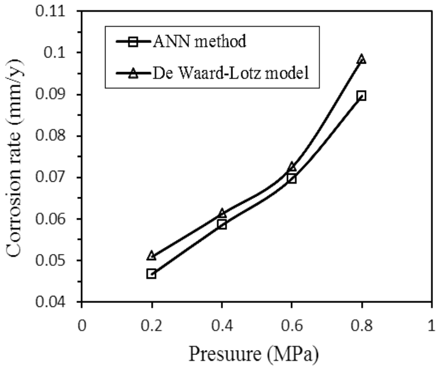

Fig. 6 Corrosion rate (mm/year) obtained from static test at 45°C.

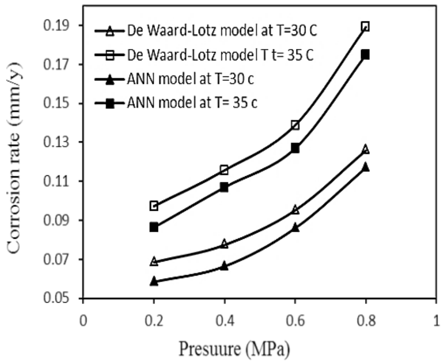

Fig. 7 Corrosion rate obtained from immersion static test at various temperatures.

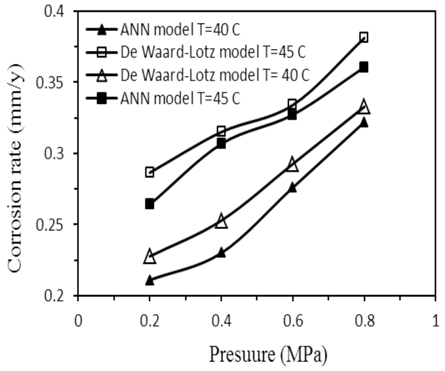

Fig. 8 Corrosion rate obtained from immersion static test at various temperatures.

As shown in Table 2, it is noticeable that NaCl has an effect on the CO_2 corrosion state. The reaction between NaCl and CO_2 is given as follows (Hamidi et al., 2017):

$NaCl + CO_2 \rightarrow Na_2CO_3 + Cl^-$ (10)

The general CO_2 corrosion rate of carbon steel significantly decreases with increasing NaCl concentration. Crude oils contain sulfur heteroatoms in the form of elemental sulfur (S), dissolved hydrogen sulfide (H_2S), carbonyl sulfide (COS), inorganic forms, and, most importantly, organic forms in which sulfur atoms are positioned within organic hydrocarbon molecules. The reaction between dissolved CO_2 and H_2S gases can form carbonyl sulfide and water (Cao et al., 2023):

$H_2S + CO_2 \Leftrightarrow H_2O + COS$(11)

High temperatures have the effect of changing sulfur from a non-reactive or poorly reactive form into a highly reactive one. This is because CO_2 and H_2S, when dissolved, react and form solid sulfur layers. Since a solid sulfur layer (composed of iron rust from API X60 carbon steel and solid sulfur) is brittle, the vibration process affects the corrosion product, causing it to exfoliate easily, which leads to increased corrosion rates.

As the temperature rises, the corrosion rate increases because higher temperatures accelerate all electrochemical corrosion processes, including CO_2 dissociation, ion transport of species, and chemical reactions. CO_2 gas dissolved in water forms carbonic acid (H_2CO_3), releasing H+ ions. Carbonic acid is a weak and unstable acid, and the release of H+ ions acidifies the crude oil solution, increasing the rate of corrosion. Additionally, crude oil contains some H_2S, which is considered an additional source of hydrogen ions during tests, thus promoting the corrosion process, especially at low pressure and temperature.

Generally, the corrosion rate increases with the rise in CO_2 partial pressure for both static and vibrational conditions. However, it has been found that the vibration process has little effect on the corrosion rate at lower pressures but becomes more significant as the CO_2 partial pressure increases.

On the other hand, as indicated in Table 3, when the partial pressure of CO_2 dissolved in crude oil increases, it reduces the crude oil's viscosity, which affects the results. The enhancement of asphalt precipitation may be due to chemical reactions between the injected CO_2 and water, leading to the formation of carbonic acid, which destabilizes asphalt. The decrease in pH may reduce asphalt stability, causing serious damage through asphalt precipitation. Additionally, the vibration process can lead to premature coking and asphalt deposition in crude oil, enhancing the separation process, which impacts the corrosion process (Fang et al., 2013; Fetisov et al., 2018).

As indicated in Figures 8-11, the corrosion rates for static and vibrational conditions at 0.2 MPa and T = 30°C are 0.0485 and 0.0552 mm/year, respectively. This shows that vibration increases the corrosion rate by (0.0552/0.0485) × 100% = 1.06%. The values obtained at 0.2 MPa and T = 45°C are 0.2881 and 0.3084 mm/year, respectively, indicating an increase of (0.3084/0.2881) × 100% = 1.07%. The corrosion rates for static and vibrational conditions at 0.8 MPa and T = 30°C are 0.1159 and 0.1227 mm/year, respectively, showing an increase of (0.1227/0.1159) × 100% = 5.86%. The values obtained at 0.8 MPa and T = 45°C are 0.3656 and 0.3829 mm/year, respectively, reflecting an increase of (0.3829/0.3656) × 100% = 4.73%. Other temperatures and partial CO_2 pressures show similar results.

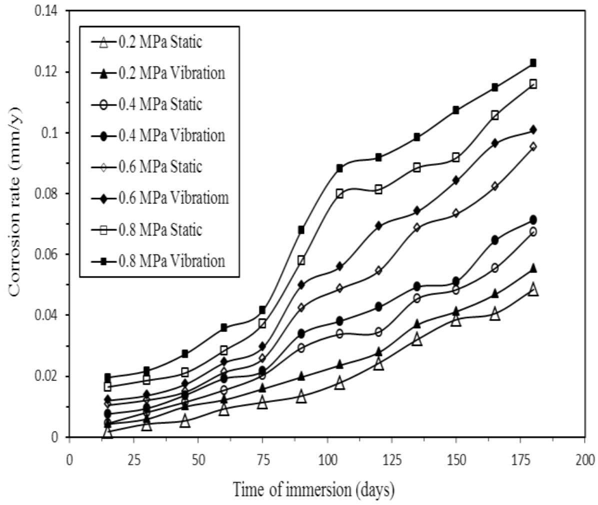

Fig. 9 Corrosion rate (mm/year) obtained from static and vibration corrosion test at 30°C

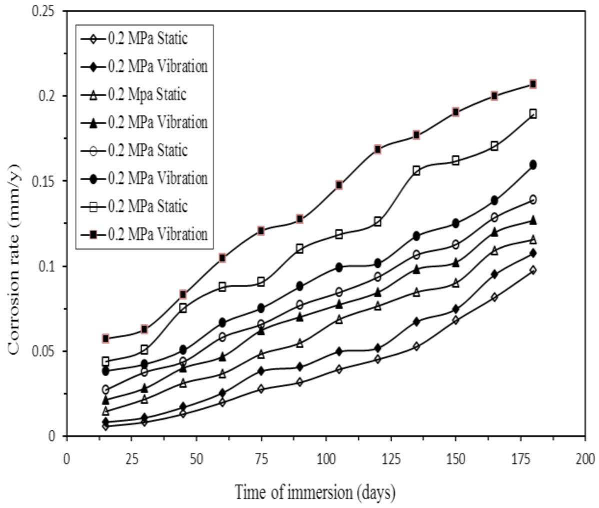

Fig. 10 Corrosion rate (mm/year) obtained from static and vibration corrosion test at 35°C

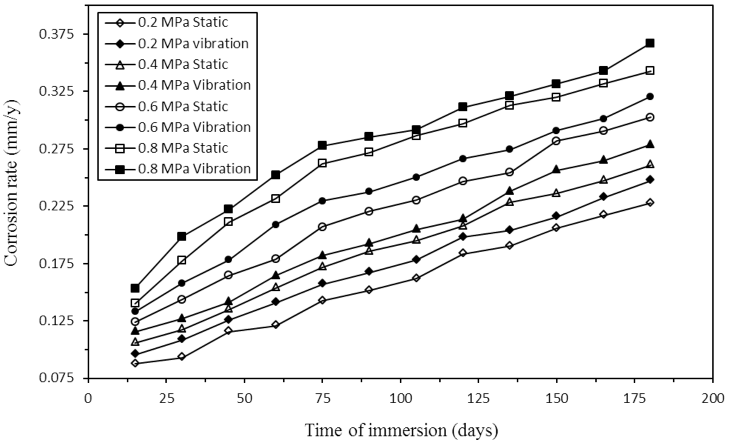

Fig. 11 Corrosion rate (mm/year) obtained from static and vibration corrosion test at 40°C.

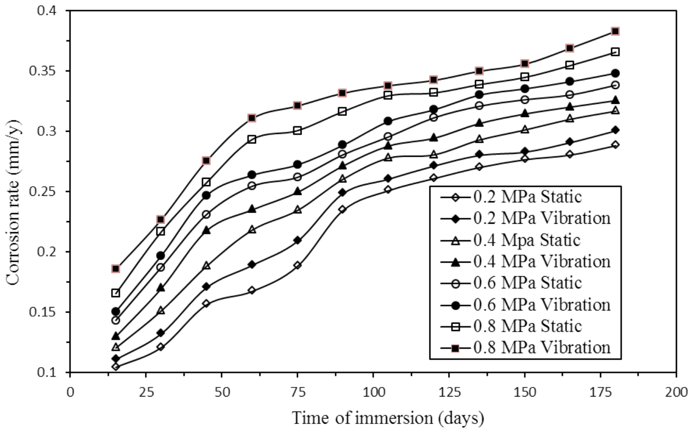

Fig. 12 Corrosion rate (mm/year) obtained from static and vibration corrosion test at 45°C.

CONCLUSION

Using a self-assembled test rig, the effect of CO_2 partial pressure on the corrosion of API 5L X60 pipeline steel was studied in simulated crude oil through corrosion coupon testing and corrosion morphology observations. When compared to values obtained from the ANN model, the CO_2 corrosion rates derived from the 1991 De Waard-Lotz-Milliams correlation under varying temperatures and CO_2 partial pressures exhibit a fair degree of accuracy. The corrosion rate increases with the rise in CO_2 partial pressure in both static and vibrational conditions. However, it was found that the vibration process has little effect on the corrosion rate at lower pressures, but its influence increases with higher CO_2 partial pressures. At constant vibration and CO_2 partial pressure, with increasing temperature, the corrosion rate increases uniformly by a constant percentage greater than 1%. Conversely, at constant vibration and temperature, with increasing CO_2 partial pressure, the corrosion rate increases uniformly by a constant percentage less than 1%.

REFERENCES

Al-Hashimy, Z. I., Al-Kayiem, H. H., & Time, R. W. (2016).Experimental investigation on the vibration induced by slug flow in horizontal pipe.*ARPN Journal of Engineering and Applied Sciences*, *11*(20).

Amarasinghe, W., Fjelde, I., &Guo, Y. (2021). CO2 dissolution and convection in oil at realistic reservoir conditions: A visualization study. *Journal of Natural Gas Science and Engineering*, *95*.https://doi.org/10.1016/j.jngse.2021.104113

American society for testing materials ASTM. (1999). ASTM G1-90: Standard Practice for Preparing , Cleaning , and Evaluating Corrosion Test. *Significance*, *90*(Reapproved).

ASTM G31 – 72. (2004). ASTM G31: Standard Practice for Laboratory Immersion Corrosion Testing of Metals. *ASTM International*, *Reapproved*.

Cao, X., Feng, Q., &Ji, Y. (2023).Effect of Interaction between Carbon Dioxide and Fluid Phase/Rock Interface on Carbon Dioxide Storage.*Processes*, *11*(12).https://doi.org/10.3390/pr11123331

Christopher L., (2010). *Artificial neural network for behavior learning from meso-scale simulations, application to multi-scale multimaterial flows* (Master's thesis, The University of Iowa).

Dai, H. L., Wang, L., Qian, Q., &Gan, J. (2012).Vibration analysis of three-dimensional pipes conveying fluid with consideration of steady combined force by transfer matrix method.*Applied Mathematics and Computation*, *219*(5).https://doi.org/10.1016/j.amc.2012.08.081

deWaard, C., Lotz, U., &Milliams, D. E. (1991). Predictive model for CO2 corrosion engineering in wet natural gas pipelines.*Corrosion*, *47*(12). https://doi.org/10.5006/1.3585212

Elliot, J. R., & Lira, C. T. (2012). Introductory Chemical Engineering Thermodynamics.*Journal of Materials Processing Technology*, *1*(1).

Fang, H., Brown, B., &Nešić, S. (2013). Sodium chloride concentration effects on general CO2 corrosion mechanisms. *Corrosion*, *69*(3).https://doi.org/10.5006/0222

Fetisov, E. O., Shah, M. S., Knight, C., Tsapatsis, M., &Siepmann, J. I. (2018).Understanding the Reactive Adsorption of H2S and CO2 in Sodium-Exchanged Zeolites.*ChemPhysChem*, *19*(4).https://doi.org/10.1002/cphc.201700993

Gatto, A., Cappelletti, C., Defanti, S., &Fabbri, F. (2023). The Corrosion Behaviour of Additively Manufactured AlSi10Mg Parts Compared to Traditional Al Alloys. *Metals*, *13*(5).https://doi.org/10.3390/met13050913

Guang Z., Api Specification 5L, Line pipe, 46 th Edition, (API Pub.,2018).

Hamidi, H., Mohammadian, E., Haddad, A. S., Rafati, R., Azdarpour, A., Ghahri, P., Pradana, A. P., Andoni, B., &Akhmetov, C. (2017). Effects of ultrasonic waves on carbon dioxide solubility in brine at different pressures and temperatures.*Petroleum Science*, *14*(3).https://doi.org/10.1007/s12182-017-0165-2

Jones, D. (1996). Principles and Prevention of Corrosion.*Materials & Design*, *14*(3).

Kermani, M. B., &Morshed, A. (2003).Carbon dioxide corrosion in oil and gas production - A compendium.*Corrosion*, *59*(8).https://doi.org/10.5006/1.3277596

Li, H. B., Yang, Z. M., Li, R. S., Zhou, T. Y., Guo, H. K., Liu, X. W., Dai, Y. X., Hu, Z. G., &Meng, H. (2021). Mechanism of CO2 enhanced oil recovery in shale reservoirs. *Petroleum Science*, *18*(6).https://doi.org/10.1016/j.petsci.2021.09.040

Lin, H.-T., Lo, C.-M., & Lin, M.-D. (2017). *Application of Artificial Neural Networks on Predicting Corrosion Rates of Carbon Steel in Taiwan Industrial Zones*. https://doi.org/10.2991/msam-17.2017.63

Lotz, U. (1993). Prediction of CO2 Corrosion of Carbon steel. *NACE CORROSION/93, paper 69*.

Mamoon, A., Audu, A., &Yunusa, N. N. (2023).Predictive Model for Corrosion Rate of Mild Steel using Artificial Neural Network.*International Journal of Material Science and Engineering*, *09*(3).https://doi.org/10.14445/23948884/ijmse-v9i3p101

Nesic, S., &Vrhovac, M. (1999).A neural network model for CO2 corrosion of carbon steel.*Journal of Corrosion Science and Engineering*, *1*.

Palmer, D. A., & van Eldik, R. (1983). The Chemistry of Metal Carbonato and Carbon Dioxide Complexes.*Chemical Reviews*, *83*(6). https://doi.org/10.1021/cr00058a004

Ziegler, K. J., Hanrahan, J. P., Glennon, J. D., & Holmes, J. D. (2003). Producing “pH switches” in biphasic water-CO2 systems. *Journal of Supercritical Fluids*, *27*(1).https://doi.org/10.1016/S0896-8446(02)00231-0